
Pocket-Dentist: On-Device Dental Image Understanding via Efficient Multimodal Large Language Models

Kai Bian^{*1} Xucheng Guo^{*2} Bin Chen³ Lingyan Ruan³ Yiran Shen² Ting Dang³ Hong Jia¹

Abstract

Evaluations of dental vision–language models remain fragmented across datasets, task definitions and metrics, and often ignore their computational cost. This limits their widespread deployment for dental screening outside specialist centres, where timely inference, limited hardware, and local handling of patient images are vital for practical, privacy-preserving clinical prescreening. Here we present Pocket-Dentist, an efficiency-aware benchmark for dental multimodal question answering that brings together three datasets spanning $\sim 1,159$ patients, five task types and seven metrics. Across typical 14 VLMs, our results reveals an interesting observation: compact VLMs (e.g., 2B-parameter models) outperform larger VLMs in accuracy while requiring substantially lower computational costs in dental image understanding. Deployed locally on an iPhone 17 Pro, our finetuned compact VLM Pocket-Dentist-2B processed each sample in 4.31 s, reducing latency by 4.9-fold and memory use by 2.3-fold compared with a 7B baseline.

1. Introduction

Oral diseases are among the most prevalent chronic health conditions globally, affecting approximately 3.7 billion people worldwide (Bernabe et al., 2025). In remote and underserved communities, patients frequently lack access to even basic oral health screening, let alone specialist diagnosis. This access gap is also an efficiency problem: preliminary screening must be delivered with limited clinical labor, intermittent connectivity, low-cost hardware, and minimal turnaround time. If visual AI models can run directly on widely available mobile devices, dental screening could reach communities that currently lack access to specialist care.

¹The University of Auckland, New Zealand ²Shandong University, China ³The University of Melbourne, Australia. Correspondence to: Hong Jia <hong.jia@auckland.ac.nz>.

In practice, dental image understanding is not a single-image, single-label problem. Dental care relies on heterogeneous visual evidence, including panoramic radiographs and intraoral photographs, and the relevant outputs range from short answers and diagnostic categories to captions and structured reports. Yet current dental AI evaluation largely studies these pieces in isolation: datasets are usually modality-specific, task definitions are not standardized across resources, and benchmark results rarely indicate whether a model that performs well in one setting remains reliable under another (Uribe et al., 2024; Li et al., 2026). This fragmentation becomes more consequential when efficiency is considered. A model intended for practical dental QA must be evaluated not only for answer quality, but also for adaptation cost, structured-output reliability, memory use, latency, and independence from cloud inference. Existing work, therefore, leaves open a central question: *whether efficient multimodal QA models can achieve reliable dental image understanding across diverse modalities and tasks while remaining feasible for resource-constrained mobile deployment.*

Efficiency is therefore a deployment requirement rather than a secondary optimization for this application. In underserved and rural screening scenarios, reliable connectivity cannot be assumed, and cloud-based multimodal QA requires transmitting patient dental images to remote servers, raising both availability and privacy concerns. On-device inference addresses these constraints by keeping data local and enabling offline, low-latency screening, but it also introduces strict memory, compute, and thermal budgets. These constraints motivate compact VLMs and make it necessary to evaluate dental QA models not only by answer quality, but also by whether they can operate within the resource envelope of a mobile device.

To address these gaps, we introduce Pocket-Dentist (Figure 1), an efficiency-aware multimodal QA benchmark and evaluation framework for dental VLMs. Pocket-Dentist formulates dental image understanding as a unified multimodal QA problem in which models are evaluated across heterogeneous imaging modalities, multiple clinical question types, structured output requirements, adaptation regimes, and mobile deployment constraints. We instantiate this setting

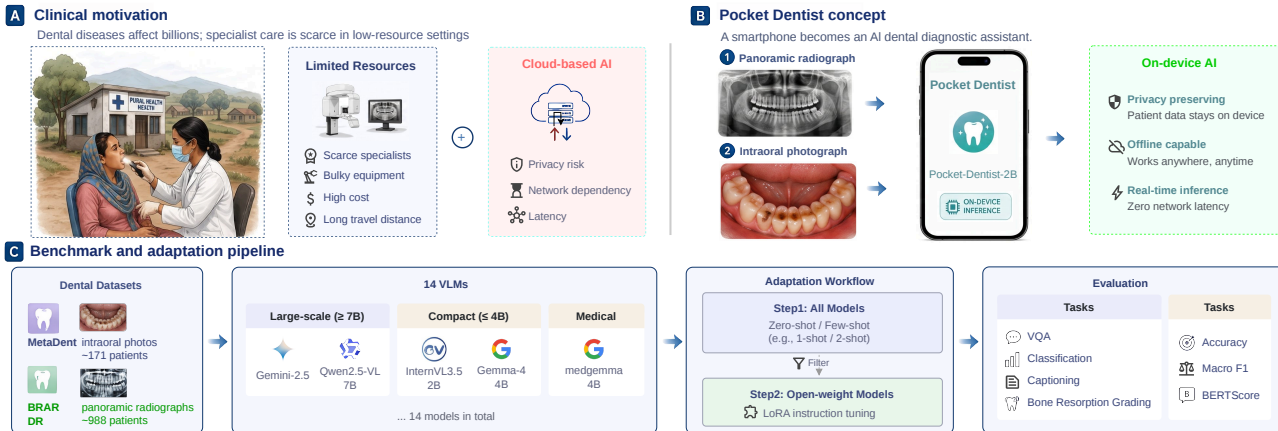


Figure 1. Overview of the Pocket-Dentist pipeline. We benchmark 14 VLMs across three dental datasets under zero-shot, few-shot, and LoRA settings, identify InternVL3.5-2B as the best-performing compact VLM, and deploy it on an iPhone 17 Pro for on-device local inference.

by curating three heterogeneous dental datasets into standardized prompt–response QA pairs through task-specific reformulation, LLM-assisted conversion, and manual quality review, yielding a unified evaluation protocol across all tasks. We evaluate 14 representative VLMs under zero-shot, few-shot, and LoRA instruction-tuning settings, characterizing the accuracy–efficiency trade-off from 1B to 32B parameters, and we deploy a LoRA-tuned compact model on an iPhone 17 Pro with on-device inference.

Our main contributions are:

- We curate Pocket-Dentist, a multimodal dental QA benchmark that unifies three datasets across panoramic radiographs and intraoral photographs, covering ~1,159 patients, five clinical question types, and seven evaluation metrics.
- We propose an efficiency-aware evaluation protocol that unifies heterogeneous dental resources through shared task definitions, structured output schemas, and seven complementary metrics spanning answer quality, adaptation cost, output reliability, memory usage, and inference latency.
- We conduct an efficiency-aware evaluation of 14 VLMs, characterizing the accuracy–efficiency trade-off across model scales. Under a uniform LoRA budget, compact adapted VLMs become competitive with larger open-weight models, and we deploy Pocket-Dentist-2B locally on an iPhone 17 Pro with 4.31 s per-sample latency, a 4.9× reduction relative to the 7B baseline.

2. Related Work

Medical VLMs. Medical vision–language models have progressed from task-specific medical VQA datasets and

benchmarks for medical visual question answering (He et al., 2020; Zhang et al., 2023) to more general-purpose medical vision–language models such as LLaVA-Med (Li et al., 2023) and Med-Flamingo (Moor et al., 2023) that leverage large-scale medical image–text pretraining. Recent work in medical AI has also emphasized clinical alignment, safety, and human evaluation as prerequisites for reliable deployment (Singhal et al., 2023). However, medical VLM evaluation remains concentrated on radiology and pathology. Dentistry differs from these domains in image acquisition, anatomical structure, annotation conventions, and potential mobile screening workflows, yet it has received limited attention as a multimodal VLM benchmark domain. As a result, it remains largely unclear how current VLMs handle dental imaging tasks or whether performance patterns observed in radiology and pathology benchmarks generalize to dental image understanding.

Dental AI benchmarks. In dentistry, AI research has largely focused on task-specific models for caries detection, while recent work has highlighted the value of multimodal integration for diagnostic support (Zhang et al., 2024; Noor Uddin et al., 2025). MetaDent (Li et al., 2026) introduced a dental imaging benchmark covering VQA, captioning, and classification from expert-annotated intraoral photographs, while BRAR (Xia et al., 2025) contributed panoramic radiograph annotations for periodontal bone loss grading. These resources are valuable, but they do not by themselves define an efficiency-aware dental QA benchmark. Without such a benchmark, there is no systematic way to determine whether compact VLMs can provide reliable dental QA across diverse tasks, or to identify the accuracy–efficiency frontier that governs practical deployment decisions. More importantly, prior work has not curated heterogeneous dental datasets into a single VLM evaluation setting that jointly covers multiple modalities, task

types, adaptation regimes, structured-output reliability, and deployment efficiency.

On-device deployment and efficient QA. On-device deployment of language models has attracted increasing attention as a route toward privacy-preserving and low-latency healthcare AI (Wang et al., 2025b; Lu et al., 2025). HealthSLM-Bench (Wang et al., 2025b) evaluated text-only small language models on wearable health tasks and assessed smartphone deployment efficiency. Lu et al. (Lu et al., 2025) systematically examined the capabilities and runtime characteristics of small language models for edge deployment. More broadly, the efficient QA community has studied accuracy–efficiency trade-offs in retrieval-augmented and compute-constrained settings, but primarily for text-only models in general domains. These efforts do not address the specific demands of multimodal vision–language QA, which must process high-resolution images alongside text under tight memory and latency budgets. Our work brings this efficiency-aware QA perspective to dental VLMs by jointly evaluating answer quality, token throughput, adaptation behavior, reliability failures, and smartphone inference within the same benchmark pipeline.

3. Pocket-Dentist

3.1. Benchmark Curation

We evaluate three dental benchmarks spanning panoramic radiography and intraoral photography, covering five clinical tasks. Table 1 summarizes the dataset characteristics. The curated corpus is reformulated into standardized VLM tasks covering seven evaluation metrics. For cross-model comparison, each task is assigned a single primary metric chosen to reflect clinical priorities. Classification tasks (BRAR, DR, MetaDent) use Macro F1 rather than accuracy because the label distributions are imbalanced: a model predicting only the majority class would achieve misleadingly high accuracy while failing on clinically important minority conditions such as severe bone resorption or rare pathologies. Captioning uses BERTScore F1 (Zhang et al., 2020) instead of surface-level n -gram metrics (BLEU, ROUGE) because clinical descriptions exhibit high lexical variation—semantically equivalent reports may use different terminology, making token-overlap metrics unreliable indicators of diagnostic fidelity. VQA uses exact-match accuracy against clinician-verified reference answers, where incorrect responses (e.g., misidentifying a lesion as normal) could directly delay treatment. Formal metric definitions are provided in Appendix B. Each dataset uses its original expert-curated train/val/test split; no additional patient-level deduplication was applied.

BRAR (Xia et al., 2025) is a multimodal dataset comprising 1,104 panoramic radiographs from 1,104 patients collected

at Shanghai Stomatological Hospital between January 1 and March 31, 2025. The cohort includes adults aged 18–75 years. Bone resorption severity is graded into three levels (Grade 1/2/3) using the Bone Resorption Age Ratio (BRAR) index. After excluding radiographs with incomplete metadata, 988 images are used with 691 / 148 / 149 train / val / test splits.

MetaDent (Li et al., 2026) is a large-scale dental image resource with 60,669 images from clinical, public, and web sources. For this study, we used its expert-curated subset of 2,588 high-quality intraoral photographs (around 171 patients), each annotated with a semi-structured meta-label describing imaging perspective, anatomical focus, and observed abnormalities. The data were split into 7,238 / 906 / 2,301 training / validation / test samples across three tasks (261 test images).

The Dental Radiography (DR) dataset (IMT Kaggle Team, 2023) is a community-contributed collection of 1,269 panoramic dental X-rays hosted on Kaggle. Each image is annotated with per-object labels across four lesion categories: Cavity, Fillings, Impacted Tooth, and Implant. We derive image-level multi-label classification targets by extracting the unique set of categories present in each image. We use 1,075 / 121 / 73 train / val / test images. Because this Kaggle collection does not provide patient-level identifiers, the $\sim 1,159$ patient count reported in this paper covers only BRAR and MetaDent.

3.2. Data Processing and Task Formulation

We transform all three benchmarks into dataset-specific prompt–response pairs to support unified VLM evaluation and supervised instruction tuning.

For BRAR, we formulate a multimodal radiograph-plus-metadata classification task: each prompt presents the panoramic image together with patient-level metadata (age, gender, missing teeth, implants, residual roots, functional tooth count) and requests a single severity grade as a JSON object. To ensure reliable evaluation, we normalize predictions using a deterministic five-level fallback parser (see Appendix A for details).

For MetaDent, we instantiate three task-specific prompt–response formats from the expert-authored meta-labels via LLM-assisted conversion (Li et al., 2026): VQA (one image–question pair per sample), multi-label classification (18 dental condition categories), and clinical captioning (free-text description). To mitigate the original $\sim 7:1:1$ task imbalance in the training and validation splits, we subsample VQA to approximately 1.5 pairs per image, yielding a balanced task ratio. The test split retains the full set of QA pairs per image, since VQA accuracy is aggregated at the image level (Section 5). The classification set and a random subset of

Table 1. Summary of benchmark datasets and task formulations.

Dataset	Modality	Task	Metric	Train	Val	Test
BRAR	Panoramic Radio.	Classification	Macro F1	691	148	149
MetaDent	Intraoral Photo	VQA Captioning Classification	Accuracy BERTScore F1 Macro F1	7,238	906	2,301
DR	Panoramic Radio.	Classification	Macro F1	1,075	121	73

VQA pairs were manually reviewed, and uncertain entries were excluded.

For DR, we aggregate per-image CSV annotations to extract the unique set of lesion categories present in each image, yielding a multi-label classification target. The model is prompted to identify which of the four lesion categories (Cavity, Fillings, Impacted Tooth, Implant) are present in the panoramic radiograph, evaluated via Macro F1 and Accuracy.

3.3. Training and Decoding Protocol

Let each benchmark task be represented as a set of image-prompt-target triples $\mathcal{D}_t = \{(x_i, p_i, y_i)\}_{i=1}^{n_t}$, where x_i is a dental image, p_i is the structured task prompt, and y_i is the reference output. For a VLM with parameters θ , zero-shot decoding predicts

$$\hat{y}_i^{\text{ZS}} = \arg \max_y p_{\theta}(y | x_i, p_i). \tag{1}$$

Few-shot evaluation augments the query with a fixed exemplar set $\mathcal{E}_K = \{(x_j, p_j, y_j)\}_{j=1}^K$, shared across models for each task:

$$\hat{y}_i^{\text{FS}} = \arg \max_y p_{\theta}(y | \mathcal{E}_K, x_i, p_i). \tag{2}$$

For LoRA instruction tuning, only the low-rank adapter parameters ϕ are optimized while the base model parameters θ remain frozen:

$$\phi^* = \arg \min_{\phi} \sum_t \sum_{(x_i, p_i, y_i) \in \mathcal{D}_t} -\log p_{\theta+\Delta_{\phi}}(y_i | x_i, p_i). \tag{3}$$

The adapted model then predicts $\hat{y}_i^{\text{SFT}} = \arg \max_y p_{\theta+\Delta_{\phi^*}}(y | x_i, p_i)$.

Each model is evaluated under three settings that correspond to different levels of deployment preparation. Under the zero-shot (ZS) setting, models are evaluated without task-specific training using structured prompts and greedy decoding (`do_sample=False`) for deterministic, reproducible predictions. Under the few-shot (FS) setting, following Brown et al. (Brown et al., 2020), we evaluate 1-shot and 2-shot in-context learning with fixed exemplars shared across all models. We report both settings separately in

Table 3 to avoid post-hoc shot-count selection on the test set. We limit the evaluation to two shots because VLM context windows must accommodate both the exemplar images and the query image; moreover, recent work on health-domain SLMs (Wang et al., 2025b) observed diminishing or negative returns beyond 1–3 shots, a pattern we also observe in Section 5.1.

For LoRA instruction tuning (SFT), we apply LoRA (Hu et al., 2022) with rank $r=16$ and $\alpha=32$, targeting all linear layers. Training runs for 3 epochs with cosine learning rate scheduling (peak lr= 2×10^{-4} , warmup ratio 0.1), effective batch size 16, and gradient checkpointing. All task-specific LoRA configurations share identical hyperparameters across all three benchmarks, so differences across models reflect adaptation behavior under a controlled low-cost budget rather than task-specific tuning. All tasks use the standard next-token prediction loss. Inference uses greedy decoding throughout. All experiments are conducted on NVIDIA H100 96 GB GPUs using PyTorch 2.x and the Hugging Face transformers library.

4. Experimental Setup

4.1. Models

We benchmark 14 vision-language models in two tiers: (i) large-scale VLMs ($\geq 7\text{B}$), including three open-source models (Lingshu-32B, MedMO-8B-Next, Qwen2.5-VL-7B (Bai et al., 2025)) and two closed-source APIs (Gemini-2.5-Flash, GPT-4o-mini); and (ii) compact VLMs ($\leq 4\text{B}$), including seven general-purpose models (Qwen3-VL-4B, gemma-4-E4B-it (Google DeepMind, 2026; Gemma Team et al., 2024), InternVL2.5-4B (Wang et al., 2025a), SmolVLM2-2.2B (Marafioti et al., 2025), InternVL3.5-2B, gemma-4-E2B-it, InternVL3.5-1B) and two medical-domain models pre-trained on biomedical corpora (medgemma-4b-it, paligemma2-3b-mix-448). This model pool is chosen to support efficiency-aware comparison across parameter scale, access type, and pretraining source.

4.2. On-Device Deployment Setup

To assess systems-level feasibility for on-device deployment, we deploy the top-performing LoRA-tuned VLMs

on an iPhone 17 Pro (A19 Pro SoC, 12 GB Unified Memory). All models are quantized to GGUF Q4_K_M (4-bit) and executed via `llama.cpp` (Gerganov, 2023) mapped to the Metal GPU API through a native Swift `LocalLLMClient` package. This on-device architecture keeps all inference local to the device, avoiding the privacy and latency concerns inherent in cloud-based deployment (Das et al., 2025; Lu et al., 2025). Models are side-loaded to the app’s Documents directory and loaded into Unified Memory for hardware-accelerated inference.

We deploy three models to quantify the efficiency–capability frontier: Pocket-Dentist-2B (InternVL3.5-2B + LoRA, our best overall compact VLM), InternVL2.5-4B, and Qwen2.5-VL-7B (7B baseline). The iPhone 17 Pro was selected because its 12 GB Unified Memory can accommodate the 7B baseline (6.03 GB). However, Pocket-Dentist-2B itself requires only 2.62 GB RAM, placing it well within the capability of mid-range devices with 4 GB+ memory (e.g., recent Android phones in the \$150–200 range), substantially lowering the hardware barrier relative to the test platform used in this study.

5. Results

5.1. Zero-Shot Fragility and Few-Shot Limits

Table 2 reports zero-shot performance across all 14 models.

Zero-shot performance. Under zero-shot evaluation, no model is consistently best across all metric columns. Gemini-2.5-Flash achieves the best BRAR F1 (0.411), MetaDent VQA accuracy (0.729), and classification F1 (0.412), while Lingshu-32B leads DR F1 (0.380). Among compact models, performance is fragmented across different tasks: gemma-4-E4B-it leads DR Acc (0.219), gemma-4-E2B-it leads BRAR Acc (0.564), illustrating that no single model—large or compact—dominates across all tasks. These results indicate that zero-shot evaluation alone is not a reliable basis for dental deployment.

Few-shot performance. Table 3 reports 1-shot and 2-shot performance separately. Moving from ZS to 1-shot, DR classification improves moderately (large-VLM mean: 0.435 vs. 0.249 ZS), suggesting that in-context exemplars help anchor lesion category boundaries. MetaDent VQA also benefits (compact-VLM mean: 0.539 vs. 0.456 ZS). However, moving from 1-shot to 2-shot shows mixed or declining gains on most metrics, consistent with HealthSLM-Bench (Wang et al., 2025b), which observed diminishing returns beyond 1–3 shots in health domains. Notably, several models report identical BRAR accuracy under the few-shot settings (e.g., 0.564 in FS-2); confusion-matrix inspection reveals that these models collapse to predicting only the majority class (Grade 2, which constitutes 84 of 149 test samples), yielding an accuracy equal to the majority-class prior rather than

reflecting genuine discriminative ability. Detailed metric definitions are provided in Appendix B.

5.2. Compact Adaptation Under a Uniform LoRA Budget

Table 4 presents LoRA fine-tuning results across all 12 open-weight models. We focus on best-in-class comparisons rather than tier-level averages, since the large-VLM tier is heterogeneous (two of three models exhibit format collapse on classification; see Section 5.4).

Effect of dental-domain adaptation. Under LoRA instruction tuning, compact VLMs improve substantially on most tasks. InternVL3.5-2B (2B) achieves the best BRAR accuracy (0.651 vs. 0.584) and the best BRAR F1 (0.633 vs. 0.497) among all open-weight models. On DR classification, gemma-4-E4B-it (4B) achieves the best Macro F1 (0.759), surpassing Lingshu-32B (0.651). On MetaDent, InternVL3.5-2B achieves the best captioning score (0.286 vs. Lingshu-32B’s 0.244). The largest adaptation gain appears in DR classification: zero-shot Macro F1 averages 0.189 across all 14 models; after LoRA, gemma-4-E4B-it reaches 0.759 F1, demonstrating that multi-label lesion classification can be reliably learned with lightweight domain adaptation.

Comparison with larger open-weight models. Under the uniform low-cost adaptation budget ($r=16$, 3 epochs), compact models can match or exceed much larger ones on the majority of tasks. InternVL3.5-2B matches or outperforms larger open-weight models (7B–32B) on 4 of 5 primary metrics. Relative to closed-source APIs, InternVL3.5-2B exceeds Gemini-2.5-Flash’s best zero-shot BRAR F1 (0.633 vs. 0.411) and GPT-4o-mini’s captioning score (0.286 vs. 0.242). On DR classification, the best LoRA-tuned compact model (gemma-4-E4B-it, F1 0.759) substantially exceeds the best closed-source zero-shot result (Gemini-2.5-Flash ZS F1 0.317). However, we cannot rule out that a higher-rank or longer-schedule configuration would close this gap for large models.

Role of medical pre-training. medgemma-4b-it and paligemma2-3b-mix-448, both pre-trained on biomedical corpora, do not consistently outperform general-purpose models of comparable size after SFT. paligemma2-3b-mix-448 collapses to near-zero on BRAR after LoRA (Acc/F1 = 0.000). medgemma-4b-it is competitive on BRAR (F1 0.439) but lags behind gemma-4-E4B-it and InternVL3.5-2B on DR and captioning tasks. One possible explanation is that broad biomedical pre-training may not sufficiently cover dental-specific visual patterns, acquisition geometry, and structured output conventions, whereas LoRA adaptation directly aligns the model with the curated dental task distribution.

Table 2. Performance of large-scale and compact VLMs under zero-shot (ZS) setting on BRAR, DR, and MetaDent benchmarks. Best result across all models is in **bold**, second-best is underlined.

Model		BRAR		DR		MetaDent		
		Acc (↑)	F1 (↑)	F1 (↑)	Acc (↑)	VQA (↑)	Cap (↑)	Cls (↑)
Large VLMs (ZS)	Lingshu-32B	0.490	<u>0.392</u>	0.380	0.082	<u>0.660</u>	0.196	<u>0.325</u>
	MedMO-8B-Next	0.255	0.191	0.210	0.041	0.387	0.135	0.056
	Qwen2.5-VL-7B	0.255	0.160	0.217	0.014	0.620	0.200	0.184
	gemini-2.5-flash	0.456	0.411	0.317	<u>0.178</u>	0.729	0.194	0.412
	gpt-4o-mini	<u>0.557</u>	0.239	0.123	0.041	0.600	0.242	0.286
	<i>Mean</i>	<i>0.403</i>	<i>0.279</i>	<i>0.249</i>	<i>0.071</i>	<i>0.599</i>	<i>0.193</i>	<i>0.253</i>
Compact VLMs (ZS)	Qwen3-VL-4B	0.436	0.369	0.100	0.014	0.620	<u>0.232</u>	0.298
	gemma-4-E4B-it	<u>0.557</u>	0.239	0.270	0.219	0.580	0.168	0.254
	InternVL2.5-4B	0.295	0.195	0.078	0.027	0.520	0.166	0.116
	medgemma-4b-it	0.443	0.330	<u>0.350</u>	0.068	<u>0.660</u>	0.168	0.139
	paligemma2-3b-mix-448	0.086	0.053	0.000	0.000	<u>0.000</u>	0.000	0.000
	SmolVLM2-2.2B	0.544	0.292	0.000	0.000	0.000	0.100	0.158
	InternVL3.5-2B	0.537	0.259	0.287	0.082	0.560	0.173	0.187
	gemma-4-E2B-it	0.564	0.240	0.000	0.000	0.640	0.140	0.190
	InternVL3.5-1B	0.228	0.219	0.317	<u>0.178</u>	0.520	0.149	0.146
<i>Mean</i>	<i>0.410</i>	<i>0.244</i>	<i>0.156</i>	<i>0.065</i>	<i>0.456</i>	<i>0.144</i>	<i>0.154</i>	

5.3. On-Device Deployment Feasibility

Table 5 reports the latency and resource utilization of top-performing LoRA-tuned VLMs deployed on an iPhone 17 Pro (12 GB Unified Memory) via on-device Metal-accelerated inference (cf. Appendix C). This deployment experiment is not intended as a clinical validation study; it tests whether benchmark-competitive compact VLMs can satisfy the memory and latency constraints of local mobile inference.

The deployment results reveal a clear accuracy–efficiency trade-off. Pocket-Dentist-2B (InternVL3.5-2B + LoRA) reduces end-to-end latency from 21.13 s for the 7B baseline to 4.31 s per sample—a 4.9× reduction—while reducing memory use from 6.03 GB to 2.62 GB (2.3× reduction). This places the benchmark-competitive compact model well within the memory budget of the test device and substantially lowers the cost of local inference. The 4B mid-point (InternVL2.5-4B) achieves 6.58 s latency with 3.08 GB RAM, providing an intermediate operating point on the accuracy–efficiency frontier.

Token efficiency. On-device profiling reveals that all three models consume identical prompt budgets (~346 input tokens averaged across tasks), as they share the same structured prompts. Output token counts are also comparable (PD-2B: 97, InternVL2.5-4B: 93, Qwen2.5-VL-7B: 110 tokens per sample), indicating that the compact model produces answers of comparable length. The efficiency gap, therefore, arises from throughput: Pocket-Dentist-2B generates output at 30.6 tokens/s versus Qwen2.5-VL-7B’s 9.2 tokens/s—a 3.3× improvement in token-generation efficiency. All throughput figures (ITPS, OTPS) are reported

as the mean of per-sample ratios rather than the ratio of aggregated totals (see Appendix C for the full aggregation protocol). This demonstrates that compact LoRA-adapted models do not sacrifice answer length for speed; they produce comparable output while requiring substantially fewer compute resources per token.

Beyond raw performance, this on-device deployment approach offers practical advantages relevant to resource-constrained settings: (i) patient privacy—dental images containing identifiable intraoral features remain on the device, mitigating data-exposure risks inherent in cloud-based inference; (ii) network independence—the system functions in offline settings common to rural clinics and mobile dental outreach programs. Combined with the benchmark results showing that Pocket-Dentist-2B matches or exceeds closed-source API performance on the majority of metrics after SFT (Section 5.2), these results demonstrate the feasibility of local on-device inference for dental image understanding (see Figure 2 in Appendix C for the on-device evaluation interface).

5.4. Output Reliability and Failure Modes

Deployment-oriented evaluation must account for output reliability, not just task accuracy. We observe two distinct failure modes across our benchmark.

Format collapse. Among the large-scale models, Lingshu-32B and MedMO-8B-Next exhibit clear format-collapse behavior after LoRA adaptation. Both produce classification F1 = 0.000 because they generate free-form text instead of the expected JSON array of category IDs. Under the uniform adaptation budget ($r=16$, 3 epochs), these larger

On-Device Dental Image Understanding via Efficient Multimodal Large Language Models

Table 3. Performance under 1-shot (FS-1) and 2-shot (FS-2) few-shot settings on BRAR, DR, and MetaDent benchmarks. Best result across all models is in **bold**, second-best is underlined.

Model		BRAR		DR		MetaDent		
		Acc (\uparrow)	F1 (\uparrow)	F1 (\uparrow)	Acc (\uparrow)	VQA (\uparrow)	Cap (\uparrow)	Cls (\uparrow)
Large VLMs (FS-1)	Lingshu-32B	0.195	0.126	0.511	0.041	<u>0.780</u>	0.160	0.105
	MedMO-8B-Next	0.174	0.099	<u>0.532</u>	0.014	0.560	0.160	0.026
	Qwen2.5-VL-7B	0.309	0.237	<u>0.173</u>	0.027	0.580	0.210	0.187
	gemini-2.5-flash	0.383	0.338	0.457	0.278	0.796	0.207	0.404
	gpt-4o-mini	0.544	<u>0.314</u>	0.503	<u>0.151</u>	0.560	0.224	<u>0.295</u>
	<i>Mean</i>	<i>0.321</i>	<i>0.223</i>	<i>0.435</i>	<i>0.102</i>	<i>0.655</i>	<i>0.192</i>	<i>0.203</i>
Compact VLMs (FS-1)	Qwen3-VL-4B	0.181	0.117	0.445	0.096	0.660	<u>0.222</u>	0.282
	gemma-4-E4B-it	0.510	0.260	0.182	0.041	0.640	<u>0.190</u>	0.249
	InternVL2.5-4B	0.195	0.133	0.324	0.041	0.580	0.167	0.097
	medgemma-4b-it	0.174	0.100	0.319	0.123	0.700	0.207	0.134
	paligemma2-3b-mix-448	0.170	0.097	0.000	0.000	0.000	0.000	0.000
	SmolVLM2-2.2B	0.248	0.185	0.533	0.014	0.511	0.145	0.153
	InternVL3.5-2B	<u>0.557</u>	0.239	0.083	0.055	0.660	0.213	0.136
	gemma-4-E2B-it	0.570	0.266	0.121	0.055	0.580	0.183	0.198
	InternVL3.5-1B	0.389	0.251	0.284	0.110	0.520	0.204	0.026
<i>Mean</i>	<i>0.333</i>	<i>0.183</i>	<i>0.255</i>	<i>0.059</i>	<i>0.539</i>	<i>0.170</i>	<i>0.142</i>	
Large VLMs (FS-2)	Lingshu-32B	0.356	0.299	0.495	0.014	0.760	0.246	0.110
	MedMO-8B-Next	0.564	0.240	0.514	0.027	0.540	0.160	0.028
	Qwen2.5-VL-7B	0.315	0.255	0.136	0.000	0.540	0.195	0.119
	gemini-2.5-flash	0.383	0.342	0.547	0.208	<u>0.755</u>	0.145	0.316
	gpt-4o-mini	0.389	0.375	<u>0.533</u>	0.082	0.520	<u>0.239</u>	0.268
	<i>Mean</i>	<i>0.401</i>	<i>0.302</i>	<i>0.445</i>	<i>0.066</i>	<i>0.623</i>	<i>0.197</i>	<i>0.168</i>
Compact VLMs (FS-2)	Qwen3-VL-4B	0.315	0.310	0.391	0.082	0.560	0.228	<u>0.289</u>
	gemma-4-E4B-it	0.403	0.286	0.176	0.041	0.620	0.184	0.230
	InternVL2.5-4B	0.564	0.240	0.227	0.041	0.540	0.219	0.084
	medgemma-4b-it	<u>0.557</u>	<u>0.347</u>	0.361	0.260	0.660	0.186	0.124
	paligemma2-3b-mix-448	0.174	0.099	0.000	0.000	0.000	0.000	0.000
	SmolVLM2-2.2B	<u>0.557</u>	0.239	0.516	0.027	0.500	0.112	0.160
	InternVL3.5-2B	0.523	0.276	0.309	0.041	0.600	0.198	0.196
	gemma-4-E2B-it	0.564	0.240	0.318	0.041	0.600	0.168	0.158
	InternVL3.5-1B	0.564	0.241	0.323	<u>0.219</u>	0.580	0.184	0.026
<i>Mean</i>	<i>0.469</i>	<i>0.253</i>	<i>0.291</i>	<i>0.084</i>	<i>0.518</i>	<i>0.164</i>	<i>0.141</i>	

models exhibited structured-output instability, suggesting that their stronger text-generation priors may require higher adaptation capacity or constrained decoding to produce valid structured outputs. This pattern echoes the class-imbalance collapse documented in HealthSLM-Bench (Wang et al., 2025b). Notably, this format collapse depresses the tier-level mean comparisons in Table 4: the large-VLM classification mean (0.034) reflects failure modes rather than capability, which is why we report best-in-class comparisons in Section 5.2.

Architectural incompatibility. Under zero-shot and few-shot settings, paligemma2-3b-mix-448 cannot process MetaDent’s multi-turn prompt format (all MetaDent and DR metrics reported as 0.000). While it begins producing valid formats after LoRA adaptation, it collapses to BRAR Acc/F1 = 0.000, indicating fundamental mismatches between its fixed-resolution architecture and the task re-

quirements.

These failure cases highlight that efficiency-aware QA evaluation must account for output reliability alongside raw accuracy. For efficient deployment, these failures also represent wasted compute: models that produce unusable outputs consume the same memory and latency budget as models that produce correct answers.

5.5. Threats to Validity

We identify three threats that readers should weigh when interpreting our results.

Patient-level separation. This cannot be fully verified in MetaDent. The dataset combines images from a university dental clinic and curated web sources, with an estimated ~ 171 unique patients. Because no formal patient-level identifier is available, we cannot fully rule out patient overlap

On-Device Dental Image Understanding via Efficient Multimodal Large Language Models

Table 4. Performance of large-scale and compact VLMs under **instruction tuning (LoRA)** on BRAR, DR, and MetaDent benchmarks. Best result across all models is in **bold**, second-best is underlined.

Model		BRAR		DR		MetaDent		
		Acc (↑)	F1 (↑)	F1 (↑)	Acc (↑)	VQA (↑)	Cap (↑)	Cls (↑)
Large VLMs (LoRA)	Lingshu-32B	0.584	0.497	0.651	0.507	0.920	0.244	0.000
	MedMO-8B-Next	0.174	0.099	0.219	0.288	0.820	0.252	0.000
	Qwen2.5-VL-7B	0.564	0.421	0.605	0.521	0.840	0.237	0.101
	<i>Mean</i>	<i>0.441</i>	<i>0.339</i>	<i>0.492</i>	<i>0.439</i>	<i>0.860</i>	<i>0.244</i>	<i>0.034</i>
Compact VLMs (LoRA)	Qwen3-VL-4B	0.570	0.549	0.636	0.603	0.820	0.226	0.116
	gemma-4-E4B-it	0.550	0.423	0.759	0.712	<u>0.880</u>	0.262	0.343
	InternVL2.5-4B	0.523	0.521	0.536	0.521	0.820	0.271	0.287
	medgemma-4b-it	<u>0.624</u>	0.439	0.561	0.479	0.780	0.261	0.246
	paligemma2-3b-mix-448	0.000	0.000	0.000	0.000	0.556	0.094	0.168
	SmolVLM2-2.2B	0.537	0.508	0.395	0.260	0.780	<u>0.277</u>	0.331
	InternVL3.5-2B	0.651	0.633	<u>0.732</u>	<u>0.699</u>	0.820	0.286	0.316
	gemma-4-E2B-it	0.174	0.099	0.687	0.644	0.820	0.225	<u>0.335</u>
	InternVL3.5-1B	0.517	0.490	0.730	0.712	0.800	0.275	0.284
	<i>Mean</i>	<i>0.461</i>	<i>0.407</i>	<i>0.560</i>	<i>0.514</i>	<i>0.786</i>	<i>0.242</i>	<i>0.255</i>

Table 5. On-device deployment efficiency of VLMs on iPhone 17 Pro (MetaDent dataset, $N=30$ samples).

Dataset	Model	TTFT (s) ↓	ITPS (t/s) ↑	OET (s) ↓	OTPS (t/s) ↑	Total (s) ↓	CPU (%) ↓	RAM (GB) ↓
MetaDent	Pocket-Dentist-2B	0.76	447.95	3.55	30.58	4.31	64.06	2.62
	InternVL2.5-4B	1.64	202.80	4.94	21.09	6.58	51.22	3.08
	Qwen2.5-VL-7B	4.88	68.98	16.25	9.17	21.13	42.85	6.03

between training and test splits. BRAR, by contrast, provides verified one-patient-per-image provenance.

Clinical provenance. The DR benchmark is a community-contributed Kaggle collection without published clinical provenance, patient demographics, or inter-annotator agreement statistics. Results on this dataset should be interpreted as a proof-of-concept for VLM classification rather than clinical evidence.

Deployment hardware. All on-device measurements are collected on a single iPhone 17 Pro, chosen to accommodate the 7B baseline model (6.03 GB RAM). The actual deployed model (Pocket-Dentist-2B, 2.62 GB) has substantially lower hardware requirements and is expected to run on mid-range devices with 4 GB+ RAM, including budget Android smartphones commonly available in resource-constrained settings. Nevertheless, no cross-platform latency or thermal measurements have been conducted, and performance on lower-spec hardware remains to be validated.

6. Conclusion

We present Pocket-Dentist, an efficiency-aware multimodal QA benchmark and evaluation pipeline for dental VLMs. The benchmark standardizes three dental datasets across panoramic radiographs and intraoral photographs into a unified dental QA evaluation comprising five task types

and seven metrics. On this benchmark, zero-shot and few-shot QA performance is fragmented across tasks, whereas dental-domain LoRA adaptation enables compact VLMs—especially InternVL3.5-2B—to match or outperform substantially larger open-weight models on the majority of primary metrics under a uniform low-cost adaptation budget. Pocket-Dentist-2B achieves 4.31 s per-sample inference on an iPhone 17 Pro with fully local computation, demonstrating a 4.9× latency and 2.3× memory reduction relative to the 7B baseline while maintaining competitive QA accuracy. The benchmark does not establish clinical efficacy or safety; it provides an empirical foundation for future work on clinical validation, efficient multimodal QA in broader healthcare domains, and cross-institution deployment studies.

References

- Bai, S., Chen, K., Liu, X., Wang, J., Ge, W., Song, S., et al. Qwen2.5-VL Technical Report. arXiv preprint, 2025. <https://doi.org/10.48550/arXiv.2502.13923>.
- Bernabe, E., Marcenés, W., Abdulkader, R. S., Abreu, L. G., Afzal, S., Alhalaiqa, F. N., et al. Trends in the global, regional, and national burden of oral conditions from 1990 to 2021: A systematic analysis for the Global Burden of Disease Study 2021. *The Lancet*, 405 (10482):897–910, March 2025. ISSN 01406736. doi: 10.1016/S0140-6736(24)02811-3.
- Brown, T. B., Mann, B., Ryder, N., Subbiah, M., Kaplan, J., Dhariwal, P., et al. Language models are few-shot learners. In *Proceedings of the 34th International Conference on Neural Information Processing Systems, NIPS '20*, Red Hook, NY, USA, 2020. Curran Associates Inc. ISBN 978-1-7138-2954-6.
- Das, B. C., Amini, M. H., and Wu, Y. Security and Privacy Challenges of Large Language Models: A Survey. *ACM Computing Surveys*, 57(6):1–39, June 2025. ISSN 0360-0300, 1557-7341. doi: 10.1145/3712001.
- Gemma Team, Mesnard, T., Hardin, C., Dadashi, R., Bhupatiraju, S., Pathak, S., et al. Gemma: Open Models Based on Gemini Research and Technology. arXiv preprint, 2024. <https://doi.org/10.48550/arXiv.2403.08295>.
- Gerganov, G. llama.cpp: Llm inference in C/C++. <https://github.com/ggerganov/llama.cpp>, 2023. GitHub repository.
- Google DeepMind. Gemma 4 model card. https://ai.google.dev/gemma/docs/core/model_card_4, 2026. Last updated: 2026-04-17.
- He, X., Zhang, Y., Mou, L., Xing, E., and Xie, P. PathVQA: 30000+ Questions for Medical Visual Question Answering. arXiv preprint, 2020. <https://doi.org/10.48550/arXiv.2003.10286>.
- Hu, E. J., Shen, Y., Wallis, P., Allen-Zhu, Z., Li, Y., Wang, S., Wang, L., and Chen, W. LoRA: Low-rank adaptation of large language models. In *International Conference on Learning Representations*, 2022. URL <https://openreview.net/forum?id=nZeVKeeFYf9>.
- IMT Kaggle Team. Dental radiography dataset. Kaggle, 2023. URL <https://www.kaggle.com/datasets/imtkaggleteam/dental-radiography>.
- Li, C., Wong, C., Zhang, S., Usuyama, N., Liu, H., Yang, J., et al. LLaVA-Med: Training a Large Language-and-Vision Assistant for Biomedicine in One Day. arXiv preprint, 2023. <https://doi.org/10.48550/arXiv.2306.00890>.
- Li, M.-X., Deng, W.-H., Wu, Z.-X., Jin, C.-X., Wu, J.-M., Han, Y., et al. MetaDent: Labeling Clinical Images for Vision-Language Models in Dentistry. *Journal of Dental Research*, pp. 00220345261424242, March 2026. ISSN 0022-0345, 1544-0591. doi: 10.1177/00220345261424242.
- Lu, Z., Li, X., Cai, D., Yi, R., Liu, F., Liu, W., et al. Demystifying Small Language Models for Edge Deployment. In *Proceedings of the 63rd Annual Meeting of the Association for Computational Linguistics (Volume 1: Long Papers)*, pp. 14747–14764, Vienna, Austria, 2025. Association for Computational Linguistics. doi: 10.18653/v1/2025.acl-long.718.
- Marafioti, A., Zohar, O., Farré, M., Noyan, M., Bakouch, E., Cuenca, P., et al. SmolVLM: Redefining small and efficient multimodal models. arXiv preprint, 2025. <https://doi.org/10.48550/arXiv.2504.05299>.
- Moor, M., Huang, Q., Wu, S., Yasunaga, M., Dalmia, Y., Leskovec, J., et al. Med-flamingo: A multimodal medical few-shot learner. In Hagselmann, S., Parziale, A., Shanmugam, D., Tang, S., Asiedu, M. N., Chang, S., Hartvigsen, T., and Singh, H. (eds.), *Proceedings of the 3rd Machine Learning for Health Symposium*, volume 225 of *Proceedings of Machine Learning Research*, pp. 353–367. PMLR, December 2023.
- Murthy, R., Yang, L., Tan, J., Awalganekar, T. M., Zhou, Y., Heinecke, S., et al. MobileAIBench: Benchmarking LLMs and LMMs for On-Device Use Cases. arXiv preprint, 2024. <https://doi.org/10.48550/arXiv.2406.10290>.
- Noor Uddin, A., Ali, S. A., Lal, A., Adnan, N., Ahmed, S. M. F., and Umer, F. Applications of AI-based deep learning models for detecting dental caries on intraoral images – a systematic review. *Evidence-Based Dentistry*, 26(1):71–72, March 2025. ISSN 1462-0049, 1476-5446. doi: 10.1038/s41432-024-01089-1.
- Singhal, K., Azizi, S., Tu, T., Mahdavi, S. S., Wei, J., Chung, H. W., et al. Large language models encode clinical knowledge. *Nature*, 620(7972):172–180, August 2023. ISSN 0028-0836, 1476-4687. doi: 10.1038/s41586-023-06291-2.
- Uribe, S., Issa, J., Sohrabniya, F., Denny, A., Kim, N., Dayo, A., et al. Publicly Available Dental Image Datasets for Artificial Intelligence. *Journal of Dental Research*,

103(13):1365–1374, December 2024. ISSN 0022-0345, 1544-0591. doi: 10.1177/00220345241272052.

Wang, W., Gao, Z., Gu, L., Pu, H., Cui, L., Wei, X., et al. InternVL3.5: Advancing Open-Source Multimodal Models in Versatility, Reasoning, and Efficiency. arXiv preprint, 2025a. <https://doi.org/10.48550/arXiv.2508.18265>.

Wang, X., Dang, T., Zhang, X., Kostakos, V., Witbrock, M. J., and Jia, H. HealthSLM-Bench: Benchmarking Small Language Models for Mobile and Wearable Healthcare Monitoring. arXiv preprint, 2025b. <https://doi.org/10.48550/arXiv.2509.07260>.

Xia, Y., Li, Z., Lin, Z., Wang, S., Wang, Y., and Xie, Y. BRAR-anchored multimodal dataset of panoramic radiographs for periodontal bone resorption grading. *Scientific Data*, 13(1):89, December 2025. ISSN 2052-4463. doi: 10.1038/s41597-025-06400-y.

Zhang, J.-W., Fan, J., Zhao, F.-B., Ma, B., Shen, X.-Q., and Geng, Y.-M. Diagnostic accuracy of artificial intelligence-assisted caries detection: A clinical evaluation. *BMC Oral Health*, 24(1):1095, September 2024. ISSN 1472-6831. doi: 10.1186/s12903-024-04847-w.

Zhang, T., Kishore, V., Wu, F., Weinberger, K. Q., and Artzi, Y. Bertscore: Evaluating text generation with bert. In *International Conference on Learning Representations*, 2020. URL <https://openreview.net/forum?id=SkeHuCVFDr>.

Zhang, X., Wu, C., Zhao, Z., Lin, W., Zhang, Y., Wang, Y., et al. PMC-VQA: Visual Instruction Tuning for Medical Visual Question Answering. arXiv preprint, 2023. <https://doi.org/10.48550/arXiv.2305.10415>.

A. Prompt Templates and Output Schemas

This section details the structured input–output formats used for each benchmark.

BRAR. The prompt presents a panoramic radiograph together with patient-level metadata (age, gender, missing teeth, implants, residual roots, functional tooth count) and requests a single severity grade. The expected output is a JSON object `{"grade": k}` where $k \in \{1, 2, 3\}$. Because models produce outputs in heterogeneous formats (e.g., plain digits, JSON objects, markdown code blocks, or embedded text), we apply a five-level deterministic fallback parser: (1) pure digit match, (2) JSON parsing, (3) markdown code-block extraction, (4) regex pattern matching, and (5) first-digit heuristic.

MetaDent. Three task-specific output schemas are used. *VQA*: `{"answer": ..., "reason": ...}`. *Classification*: a JSON array of detected conditions, e.g., `[{"id": "C1", "name": "Dental caries", "evidence": "..."}]`. *Captioning*: `{"description": "..."}`.

DR. The prompt describes the four supported finding categories (Cavity, Fillings, Impacted Tooth, Implant) with radiographic definitions. The model is asked to identify which categories are present in the panoramic radiograph. The expected output is a structured JSON listing the detected categories, e.g., `{"objects": [{"label": "Cavity"}, {"label": "Fillings"}]}`.

B. Evaluation Metrics

This section provides formal definitions and clinical rationale for all evaluation metrics used in our benchmark tables. Arrows in column headers indicate optimization direction: (↑) higher is better; (↓) lower is better.

B.1. Task-Level Metrics (↑)

BRAR Accuracy / F1 (↑) evaluate three-class classification performance (Grade 1/2/3) for periodontal bone resorption grading in panoramic radiographs. Accuracy measures overall correctness, while Macro F1 accounts for class imbalance across resorption severity grades. In clinical practice, misgrading bone resorption can lead to delayed intervention in progressive periodontal disease, making higher recall—and consequently higher F1—clinically imperative.

DR Macro F1 / Accuracy (↑) evaluate image-level multi-label classification across four lesion categories (Cavity, Fillings, Impacted Tooth, Implant) in panoramic radiographs. Macro F1 is the unweighted mean of per-class F1 scores, ensuring balanced evaluation across categories regardless of prevalence. Accuracy measures the proportion of images whose predicted category set exactly matches the ground-truth set. In clinical practice, correctly identifying the types of lesions present in a radiograph is a prerequisite for appropriate treatment planning.

VQA Accuracy (↑) denotes the proportion of correctly answered visual questions, computed as exact-match accuracy against clinician-verified reference answers. In dental diagnostics, a higher VQA accuracy directly translates to more reliable triage recommendations—an incorrect answer (e.g., misidentifying a lesion as “normal”) could delay critical treatment.

Captioning BERTScore F1 (↑) calculates a semantic similarity score between generated captions and reference descriptions, computed via contextual embeddings. Unlike surface-level n -gram overlap (BLEU/ROUGE), BERTScore captures paraphrase equivalence, which is essential in clinical reporting where lexical variation is high but semantic fidelity is paramount. Higher scores indicate that the model’s narrative more faithfully conveys the clinical findings present in the radiograph.

Classification F1 (↑) represents the harmonic mean of precision and recall across 18 dental condition categories. F1 is preferred over raw accuracy because the MetaDent label distribution is heavily long-tailed: a model that predicts only the majority class achieves high accuracy but clinically dangerous low recall on rare pathologies (e.g., periapical abscess). Higher F1 ensures balanced sensitivity across both common and rare conditions.

B.2. Deployment Efficiency Metrics

TTFT (↓), OET (↓), and Total Time (↓) are latency metrics measured in seconds. In a chairside clinical workflow, the dentist awaits the model’s response while the patient is present; excessive latency disrupts the consultation flow and reduces practitioner trust. Lower values directly improve clinical usability. TTFT captures perceived responsiveness (time to first token); OET and Total Time capture end-to-end throughput for complete diagnostic output.

ITPS (↑) and OTPS (↑) are throughput metrics measured in tokens per second. Higher input throughput (ITPS) enables faster

processing of multimodal prompts containing high-resolution dental images; higher output throughput (OTPS) accelerates the generation of structured diagnostic responses. Together, they characterize the computational efficiency of the inference engine on resource-constrained mobile hardware.

CPU (↓) and RAM (↓) denote resource utilization metrics. Lower CPU usage preserves battery life and reduces thermal throttling during sustained clinical sessions. Lower RAM footprint determines deployment feasibility on devices with limited unified memory (e.g., 12 GB on iPhone 17 Pro) and leaves headroom for the host application’s UI and camera pipeline.

C. Deployment Setup and Metrics

C.1. Hardware and Software Environment

- Device: iPhone 17 Pro, iOS 26.3.1, Apple A19 Pro SoC, 12 GB Unified Memory.
- Inference Engine: llama.cpp via LocalLLMClient Swift package, mapping Metal API to GPU-accelerated inference.
- Quantization: All models converted to GGUF format with Q4_K_M (4-bit) quantization.
- Architecture: Pure on-device inference (Route A)—no network communication; models are sideloaded to the app’s Documents directory via Finder and loaded entirely into Unified Memory.

C.2. Efficiency Metrics

Following MobileAIBench (Murthy et al., 2024), we adopt:

- TTFT (s): Time-to-first-token—latency from prompt submission to first output token.
- ITPS (t/s): Input tokens per second—prompt processing throughput.
- OTPS (t/s): Output tokens per second—generation throughput.
- OET (s): Output evaluation time—wall-clock time for complete response generation.
- Total Time (s): End-to-end per-sample latency (TTFT + OET).
- CPU (%): Average CPU utilization during inference.
- RAM (GB): Peak memory allocation during model inference.

C.3. Aggregation Protocol

Latency metrics are averaged over $N = 30$ samples (10 per task \times 3 tasks). Following HealthSLM-Bench methodology, MetaDent is treated as a single data pool without task-level stratification for efficiency measurement, as latency metrics reflect computational engine characteristics rather than task-specific semantics. CPU utilization is the per-second average load; RAM is the peak allocation.

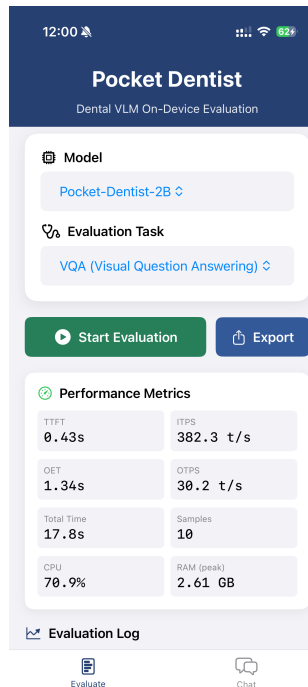


Figure 2. Pocket-Dentist iOS app running Pocket-Dentist-2B on an iPhone 17 Pro.